Enhanced Compressive Sensing Method of Moments via Physics-Aware Characteristic Modes and LSQR Solver

Yang Liu[1], Zhonggen Wang[1], Wenyan Nie[2], and Longhui Sun[1]

[1]School of Electrical and Information Engineering
Anhui University of Science and Technology, Huainan 232001, China
2023200714@aust.edu.cn, zgwang@ahu.edu.cn, 15556361695@163.com

[2]School of Mechanical and Electrical Engineering
Huainan Normal University, Huainan 232001, China
wynie5240@163.com

Abstract – To improve the computational efficiency and stability of the compressive sensing-method of moments (CS-MoM) based on characteristic mode basis functions (CMBFs) for electromagnetic scattering problems, this paper introduces an enhanced construction strategy for CMBFs. The proposed method adopts a dual strategy framework that synergistically integrates physical insight with mathematical screening, replacing the conventional approach based solely on mathematical selection. This integration significantly enhances the physical interpretability and sparsity of the resulting basis functions. In addition, the least squares QR (LSQR) iterative algorithm, which solves the problem by utilizing QR decomposition, is employed instead of the traditional LS method for the CS reconstruction problem. This replacement alleviates the detrimental effects of ill-conditioned matrices on solution stability, thereby improving the robustness and accuracy of the algorithm. Numerical results confirm that the proposed method substantially reduces computational complexity while enhancing numerical stability.

Index Terms – Characteristic mode basis functions, compressive sensing, method of moments, reconstruction algorithm.

I. INTRODUCTION

The method of moments (MoM) [1] is an effective full-wave numerical technique for solving electromagnetic scattering problems, renowned for its high accuracy and broad applicability. However, when applied to electrically large targets, the computational complexity of the resulting matrix equations increases significantly. To address this challenge, several acceleration algorithms have been proposed, including the multilevel fast multipole method [2], characteristic basis function method [3], and adaptive cross approximation [4], all aiming to reduce the matrix size or expedite the solution process. In recent years, compressive sensing (CS) [5] has been introduced into the MoM framework, offering a novel approach for the efficient solution of electromagnetic scattering problems. This integration has driven the development of CS-based MoM (CS-MoM) [6] computational models, with the core idea centered on sparsity optimization of the traditional MoM computational structure. This optimization effectively reduces the computational burden and enhances overall computational efficiency.

The CS-MoM model primarily comprises two computational frameworks. One framework targets monostatic electromagnetic scattering problems and introduces a novel excitation source construction method [7–9]. The key idea is to randomly combine incident excitations from different angles, thereby reducing the number of matrix equations that need to be solved. The other framework is designed for bistatic electromagnetic scattering [10–13], wherein CS techniques are directly integrated into the algorithmic structure of MoM. This approach transforms the full-rank matrix equations into low-dimensional underdetermined systems, significantly decreasing both the matrix filling and solution complexity.

The solution process of the second type of CS-MoM model primarily involves three key steps: constructing the sparse basis, constructing the measurement matrix, and reconstructing the current coefficients. Among these, the critical challenges lie in how to construct a sparse basis with clear physical significance and strong expressive capability, as well as how to select appropriate reconstruction algorithms to enhance computational accuracy and efficiency, both of which are central to the efficient solution of bistatic electromagnetic scattering problems using CS-MoM. Currently,

Submitted On: November 22, 2025
Accepted On: March 09, 2026

https://doi.org/10.13052/2026.ACES.J.410310

commonly used sparse bases for three-dimensional (3D) problem analysis include characteristic basis functions (CBFs) [14, 15], characteristic mode basis functions (CMBFs) [13, 16], and Krylov subspace basis functions [12, 17]. Among them, CMBFs have attracted significant attention due to their excitation-independent construction and suitability for large-scale electromagnetic scattering analysis, especially when combined with domain decomposition strategies. However, existing selection methods for CMBFs primarily rely on purely mathematical criteria [16], which may lead to redundant basis functions and reduce the efficiency of sparse representation. Moreover, many existing approaches accelerate the sparse basis construction process by eliminating basis functions associated with small-amplitude coefficients, thereby forming an overdetermined system. In such systems, ensuring the accuracy of reconstruction typically requires careful determination of the sensing matrix's column structure. Under these circumstances, classic iterative reconstruction algorithms, such as orthogonal matching pursuit (OMP) [18] or generalized OMP (gOMP) [19], often exhibit limited efficiency. To address this issue, the least squares (LS) method is adopted in conjunction with the characteristic mode-based CS-MOM (CM-CS-MoM) [13] framework to enhance the computational efficiency. Nevertheless, during the construction of the normal equations, the explicit formulation of reduced matrices may lead to ill-conditioning, adversely affecting both the stability and accuracy of the final solution.

To address the key challenges in the sparse representation and reconstruction processes described above, this study introduces improvements and optimizations from two perspectives. First, in the construction and selection of CMBFs, greater emphasis is placed on incorporating physical insights into the basis function selection process, thereby avoiding redundancy or deviation in the representation of the target's scattering field. To this end, an enhanced selection strategy that integrates physical mechanisms with mathematical criteria is proposed. By embedding the physical characteristics of current distribution into the basis selection process, the proposed method significantly improves the accuracy and sparsity of basis functions in representing electromagnetic scattering features. Second, during the reconstruction of current coefficients, the traditional LS method is replaced by the least-squares QR (LSQR) iterative algorithm. LSQR offers strong numerical stability and is well-suited to handling ill-conditioned problems, particularly in the context of high-dimensional overdetermined or underdetermined systems. It demonstrates superior reconstruction performance under such conditions. The combined effect of these two enhancements not only improves the overall computational efficiency of the CM-CS-MoM framework but also significantly enhances its robustness and adaptability.

II. THEORY

A. CM-CS-MoM framework

In the MoM, the integral equation is discretized into the following matrix equation by using the Rao-Wilton-Glisson (RWG) functions as basis functions and weighting functions:

$$\mathbf{ZI} = \mathbf{V}, \tag{1}$$

where $\mathbf{Z}$ denotes a full-rank impedance matrix of dimension $N \times N$, and N represents the number of unknowns. In addition, $\mathbf{I}$ represents the induced current to be solved, and $\mathbf{V}$ represents the incident excitation of dimension $N \times 1$. At this point, by uniformly extracting M rows from $\mathbf{Z}$ and $\mathbf{V}$, the measurement matrix $\hat{\mathbf{Z}}$ and the measurement values $\hat{\mathbf{V}}$ are constructed, respectively. The equation (1) is then transformed into the following underdetermined system:

$$\hat{\mathbf{Z}}\mathbf{I} = \hat{\mathbf{V}}. \tag{2}$$

Considering that the induced current $\mathbf{I}$, discretized using RWG basis functions, is typically not sparse, a sparse transformation is therefore required:

$$\mathbf{I} = \boldsymbol{\Psi}\boldsymbol{\alpha}, \tag{3}$$

where $\boldsymbol{\alpha}$ is the weight coefficient vector, and $\boldsymbol{\Psi}$ is the sparse basis. Therefore, substituting equation (3) into equation (2) gives:

$$\hat{\mathbf{Z}}\mathbf{I} = \hat{\mathbf{Z}}\boldsymbol{\Psi}\boldsymbol{\alpha} = \boldsymbol{\Theta}\boldsymbol{\alpha} = \hat{\mathbf{V}}, \tag{4}$$

where $\boldsymbol{\Theta}$ is defined as the sensing matrix of size $M \times N$.

Since the construction of CMBFs is independent of the excitation and allows for efficient solving, they are employed as the sparse basis for current transformation [16]. Thus, $\mathbf{I}$ is expressed as equation (5), and equation (4) transforms to equation (6):

$$\mathbf{I} = \mathbf{J}^{CM}\boldsymbol{\alpha}, \tag{5}$$

$$\hat{\mathbf{Z}}\mathbf{I} = \hat{\mathbf{Z}}\mathbf{J}^{CM}\boldsymbol{\alpha} = \boldsymbol{\Theta}\boldsymbol{\alpha} = \hat{\mathbf{V}}, \tag{6}$$

where $\mathbf{J}^{\mathrm{CM}}$ has dimensions of $N \times K$, with K representing the total number of valid modes across all blocks. The sensing matrix $\boldsymbol{\Theta}$ needs to satisfy the restricted isometry property (RIP) [20] constraint. In this case, it is sufficient to solve the optimization problem under the l_1-norm:

$$\boldsymbol{\alpha} = \arg\min \|\boldsymbol{\alpha}\|_{l1} \quad s.t\ \boldsymbol{\Theta}\boldsymbol{\alpha} = \hat{\mathbf{V}}. \tag{7}$$

It is worth noting that equation (6) forms a low-dimensional overdetermined system. At this point, the

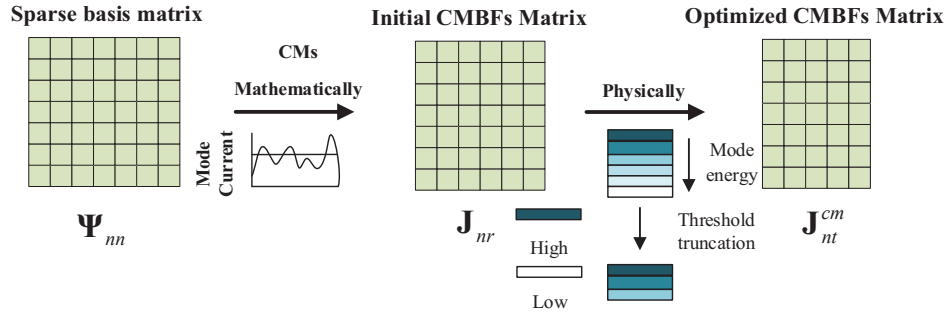

Fig. 1. Construction of CMBFs via a dual screening mechanism.

LS method can be used to replace the traditional greedy algorithm for a fast solution of the system:

$$\boldsymbol{\alpha} = (\boldsymbol{\Theta}^T \hat{\mathbf{V}})/(\boldsymbol{\Theta}^T \boldsymbol{\Theta}), \tag{8}$$

where $\boldsymbol{\Theta}^T$ is the transpose matrix of $\boldsymbol{\Theta}$.

B. Improved characteristic mode basis functions

The traditional approach for selecting CBFs primarily relies on mathematical eigenvalue decomposition. This method extracts eigenvalues from the impedance matrix through eigenvalue decomposition, and the corresponding eigenvectors are then chosen as basis functions based on these eigenvalues. From a mathematical perspective, these characteristic modes (CMs) represent inherent patterns of the scattering object. Typically, the most significant modes are selected based on the ranking of eigenvalues or mode energy. The sorting of eigenvalues is usually determined by their magnitude, with smaller eigenvalues corresponding to the characteristic modes being chosen to preserve the primary modes associated with electromagnetic scattering.

However, this method does not fully exploit the physical characteristics of the scattering object, which may result in the erroneous selection of low-energy redundant modes and the inclusion of numerical mode errors. These issues can adversely affect both the accuracy of the solution and the overall computational efficiency.

To address these limitations, a physics-informed and mathematically-guided selection strategy is proposed, which combines the electromagnetic response characteristics inherent in the physical model with the eigenvalue decomposition techniques of the mathematical model to optimize the selection of CMBFs. From a physical standpoint, modes exhibiting higher modal energy are typically associated with stronger electromagnetic responses; therefore, prioritizing modes with greater energy contributes to improved solution accuracy. By ranking characteristic modes according to their modal energies and retaining those with the highest energy, the selected basis functions are ensured to effectively represent the dominant distribution of the electromagnetic fields. As shown in Fig. 1, the process of constructing the CMBFs matrix under the dual screening of mathematical and physical principles clearly highlights the innovation of the proposed method.

From a reconstruction perspective, high-energy modes exhibit stronger physical orthogonality, leading to lower cross-correlation coefficients and enhanced sparsity concentration. From an information-theoretic viewpoint, the proposed dual-selection strategy maximizes the information entropy of the basis functions, as high-energy modes convey more scattering field information and effectively prevent the information dilution associated with low-energy modes. Modal energy directly reflects the contribution strength of the current distribution to the scattered field, thereby improving the physical interpretability of the solution. Furthermore, by reducing the number of selected modes, the proposed approach significantly enhances computational efficiency.

Specifically, from an information entropy perspective:

$$\eta(\mathbf{J}^{\mathrm{CM}}) = \sum_{i=1}^{K} P_i \log p_i \quad p_i = \frac{E_i}{\sum_{j=1}^{K} E_j}, \tag{9}$$

where $\eta(\mathbf{J}^{\mathrm{CM}})$ denotes the information entropy of the current distribution $\mathbf{J}^{\mathrm{CM}}$, which measures the uniformity of the mode energy distribution. E_i represents the energy of the ith characteristic mode, p_i denotes the proportion of the ith mode energy relative to the total energy, and K refers to the total number of modes retained.

At this stage, a physical selection mechanism is introduced to eliminate low-energy modes, effectively avoiding information redundancy and enhancing the system's information entropy, thereby achieving the goal of accelerating computational efficiency. Specifically, the modal energy is calculated as:

$$E_i = \|\mathbf{J}_i^{CM}\|^2 = \sum_{k=1}^{N_m} |\mathbf{J}_{i,k}^{CM}|, \tag{10}$$

where, $\mathbf{J}_{i,k}^{\mathrm{CM}}$ denotes the value of mode i at degree of freedom k. At this point, the index permutation mapping $\sigma : \{1,\ldots,K\} \to \{1,\ldots,K\}$ is constructed to satisfy:

$$\begin{aligned} E_{\sigma(1)} \geq E_{\sigma(1)} \geq \cdots \geq E_{\sigma(K)} \\ K = \min(|\mathbf{J}_i^e|, MaxModes). \end{aligned} \tag{11}$$

Therefore, the ordered index sequence $S = (\sigma(1), \sigma(2),\ldots,\sigma(K))$ is generated, which arranges the energy distribution in a monotonically decreasing order. In addition, *MaxModes* denotes the maximum number of modes preset for each subdomain.

Finally, the objective function for the joint physical and mathematical optimization is:

$$\Gamma = \sum_{i=1}^{N} \mathrm{II}(MS < \tau) + \beta \sum_{i=1}^{N} E_i, \tag{12}$$

where II() denotes the indicator function (which takes the value 1 when the condition is satisfied, and 0 otherwise), and β represents the weighting parameter (typically set to 1). Furthermore, the first half of the equation corresponds to numerical sparsity, while the second half represents physical significance.

C. Least square QR dissolution

In conventional CS reconstruction approaches, the LS method is frequently employed to solve for the current coefficients $\boldsymbol{\alpha}$ by minimizing the observation error, thereby enabling the recovery of the original signal.

As shown in equation (8), its analytical solution is obtained by constructing the normal equations. However, this approach suffers from numerical instability; when the columns of matrix $\boldsymbol{\Theta}$ are highly correlated, $\boldsymbol{\Theta}^T\boldsymbol{\Theta}$ may become nearly singular, resulting in an unstable solution. In addition, the requirement to store and process large-scale matrices, along with their transposes and inverses, poses significant challenges in terms of memory consumption and computational scalability, particularly for 3D electromagnetic scattering problems involving electrically large targets.

To address the aforementioned issues, this paper introduces the LSQR iterative algorithm. Rather than explicitly constructing $\boldsymbol{\Theta}^T\boldsymbol{\Theta}$, the LSQR algorithm directly performs iterations to minimize the Euclidean (L2) norm of the error:

$$\min_{\alpha} \|\boldsymbol{\Theta}\boldsymbol{\alpha} - \hat{\mathbf{V}}\|_2. \tag{13}$$

In each iteration, LSQR avoids direct matrix inversion and operates without forming $\boldsymbol{\Theta}^T\boldsymbol{\Theta}$, thereby mitigating numerical instability. It achieves this by progressively approximating the solution within a Krylov subspace framework. The k-dimensional Krylov subspace is defined as:

$$\begin{aligned} &K_k(\boldsymbol{\Theta}^T\boldsymbol{\Theta}, \boldsymbol{\Theta}^T\hat{\mathbf{V}}) \\ &\quad = span\{\boldsymbol{\Theta}^T\hat{\mathbf{V}}, (\boldsymbol{\Theta}^T,\boldsymbol{\Theta})\boldsymbol{\Theta}^T\hat{\mathbf{V}}, \ldots, (\boldsymbol{\Theta}^T\boldsymbol{\Theta})^{k-1}\boldsymbol{\Theta}^T\hat{\mathbf{V}}\}, \end{aligned} \tag{14}$$

$$r_0 = \boldsymbol{\Theta}\boldsymbol{\alpha} - \hat{\mathbf{V}}_0, \tag{15}$$

$$K_k(\boldsymbol{\Theta}^T\boldsymbol{\Theta}, \boldsymbol{\Theta}^T\hat{\mathbf{V}}), \tag{16}$$

where equation (15) represents the initial residual, while equation (16) denotes the sequence of Krylov subspaces. At the kth iteration, LSQR solves:

$$\boldsymbol{\alpha}_k = \arg\min_{\boldsymbol{\alpha}\in K_k} \|\boldsymbol{\Theta}\boldsymbol{\alpha} - \hat{\mathbf{V}}\|_2. \tag{17}$$

This iterative process converges toward the minimum residual solution without forming or storing large-scale matrix products. The use of Golub-Kahan bidiagonalization further enhances the numerical robustness by orthogonalizing the Krylov basis and avoiding loss of orthogonality due to round-off errors.

In the context of this work, integrating LSQR into the CS-MoM framework not only enhances numerical stability in the presence of ill-conditioned systems but also provides a computationally efficient pathway for solving underdetermined or overdetermined systems arising from sparse basis pruning. This contributes directly to the robustness and scalability of the proposed method, especially in scenarios involving electrically large and geometrically complex targets.

Finally, Fig. 2 presents the computational flowchart of the LSQR algorithm. Unlike the explicit matrix construction and direct solution employed in the traditional LS method, LSQR iteratively approximates the solution through successive refinements.

D. Computational complexity analysis

In this paper, the CM-CS-MoM method and the proposed approach are employed. Their computational complexity primarily arises from three components: the construction of the sparse basis, the formation of the measurement matrix, and the recovery of the sparse coefficient vector. Since both methods share the same complexity in constructing the measurement matrix, this component is excluded from the analysis.

***Construction of sparse basis*:** In the mathematical screening method, for each subdomain, a generalized eigenvalue problem is solved based on the impedance matrix, with computational complexity $O(R \cdot N^2/(\log N)^2)$, where R is the number of subdomains and N is the number of unknowns per subdomain. The basis vectors corresponding to selected eigenvalues are

Algorithm 1 LSQR Algorithm

Step 0: Initialization

$u_1 = b/\|b\|_2$, $v_1 = A^T u_1/\|A^T u_1\|_2$

$w_1 = v_1, x_0 = 0, \varphi = \|b\|_2, \rho = \|v_1\|_2$

$\beta_1 = \|b\|_2, \alpha_1 = \|A^T u_1\|_2$

for k = 1, 2, ..., max_iter:

a) Lanczos Bidiagonalization (Krylov basis):

$\beta_{k+1} u_{k+1} = A v_k - \alpha_k u_k$

$\alpha_{k+1} v_{k+1} = A^T u_{k+1} - \beta_{k+1} v_k$

b) QR Factorization (Stabilization):

$\rho_k^- = \sqrt{\rho_k^2 + \beta_{k=1}^2}$

$c_k = \rho_k / \rho_k^-, s_k = \beta_{k+1} / \rho_k^-$

$\theta_k = s_k \alpha_{k+1}, \rho_{k+1} = c_k \alpha_{k+1}$

c) Krylov Solution Update:

$w_{k+1} = (v_{k+1} - \theta_k w_k)/\rho_k^-$

$x_k = x_{k-1} + (\varphi c_k / \rho_k^-) \cdot w_{k+1}$

d) Residual Update:

$\varphi_{k+1} = \varphi s_k$

if $|\varphi_{k+1}| < tol \cdot \beta_1$: break

Fig. 2. Flowchart of LSQR algorithm.

assembled to construct the sparse basis matrix, with complexity $O(R \cdot N \cdot T)$, where T is the total number of selected characteristic modes.

In the physics-based and mathematical screening method, the complexity of computing the physical characteristic basis functions is the same as that in the mathematical screening method, up to a maximum of T_{bm} modes. The additional screening based on modal energy, along with eigenvalue filtering, has complexity $O(R \cdot N \cdot T_{bm})$.

Since sufficient accuracy can be achieved for bistatic scattering problems when $T_{bm} \leq 200$, the overall complexity of this hybrid method is significantly lower and more controllable than the purely mathematical screening method.

***Recovery sparse coefficient vector*:** Although both methods use the same linear algebra operations for current reconstruction, the physics-based and mathematical screening method has a significantly lower computational cost due to the enforced upper bound T_{bm} on the number of characteristic modes. In contrast, the mathematical screening method may select a much larger number of modes T, leading to higher complexity in matrix multiplications and inversions.

Therefore, under the same reconstruction framework, the computational complexity is $O(M \cdot T + M \cdot T^2 + N \cdot T)$ when using the LS algorithm with mathematical screening, whereas it is $O(M \cdot T_{bm} + k \cdot zzn(\boldsymbol{\Theta}) + N \cdot T_{bm})$ when employing the LSQR algorithm in combination with both mathematical and physical screening, where, k denotes the number of iterations, which is typically less than 200, and $zzn()$ represents the number of non-zero elements in the matrix. Since $T_{bm} < T$, the proposed method exhibits lower computational complexity in the reconstruction stage from an overall perspective.

III. NUMERICAL RESULTS

Different objects are simulated and analyzed to test the proposed method's effectiveness. The accuracy was evaluated using the root mean square error (RMSE) of the radar cross section (RCS), which is defined as:

$$RMSE = \sqrt{\frac{1}{N_a} \sum_{i=1}^{N_a} |RCS_{cal,i} - RCS_{ref,i}|^2}, \tag{18}$$

where $RCS_{cal,i}$ is the calculation result of the method used, $RCS_{ref,i}$ is the calculation result using MoM, and N_a is the number of sampling points.

First, the bistatic RCS of a perfectly electrically conducting (PEC) cube with an edge length of 1 meter was calculated at an incident frequency of 1 GHz, with the scattering angle observed at position $(\theta, \varphi) = (0^\circ - 360^\circ, 0^\circ)$, where θ and φ represent the azimuth and zenith angles, respectively. The surface of the cube was discretized into 21888 triangular elements. The surface electric field integral equation was discretized using RWG basis functions, resulting in 32832 unknowns. The target was partitioned into 16 blocks, each with an extension width of 0.15 times the wavelength, leading to a total of 39377 unknowns after domain expansion. In addition, during the mathematical screening process, the mode significance (MS) threshold was set to 0.001, resulting in the generation of 3196 CMs. In practice, for the CMBFM, when the extended region and the MS threshold are set to 0.1λ and 0.0001, respectively, the RMSE is 0.1 dBsm. A similar level of accuracy can also be achieved with an MS threshold of 0.002 and an extended region of 0.3λ. However, a larger extended region leads to an excessive number of unknowns on each subdomain, which significantly increases the computational time. To strike a balance between computational accuracy and efficiency, the extended region is generally set to 0.15λ, and this value is adopted consistently in all subsequent numerical examples. In the proposed method, an additional physical screening criterion was introduced, as shown in Table 1. By constraining the number of CMs generated per subdomain, the total number of CMs is effectively controlled. It can be observed that as the number of CMs increases, the

Table 1: Time and accuracy based on dual screening

	CMs count	960	1080	1200	1320	1440	1560	1680	1800	1920	2040	2160
Proposed Method	Construction time/s	33.0	33.8	35.5	37.8	40.7	43.2	44.7	46.7	48.5	50.9	53.1
	RMSE/dBsm	0.348	0.199	0.168	0.087	0.088	0.089	0.101	0.097	0.090	0.087	0.092

construction time grows accordingly, while the reconstruction error decreases. When the total number of CMs reaches 1320, the improvement in accuracy becomes marginal, indicating a saturation of the selected basis functions. Therefore, based on a trade-off between computational accuracy and efficiency, the number of CMs per subdomain was set to 110, resulting in a total of 1320 CMs. The number of CMs per subdomain is determined by the accuracy saturation behavior. When the RCS error tends to be stable, the smallest number of CMs that meets the accuracy requirement is selected. This method is objective and can be generalized to different PEC targets and mesh configurations.

To validate the advantages of the proposed method, Fig. 3 presents the solution time and reconstruction error (RMSE) under varying extraction steps for two different reconstruction approaches. The solution time includes both matrix construction and current recovery. In Fig. 3 (a), the conventional mathematical screening is employed to construct the CMBFs, while in Fig. 3 (b), the proposed dual screening strategy based on both mathematical and physical is employed.

As shown in Fig. 3 (a), when the extraction step ranges from 4 to 8, the reconstruction accuracy of the LSQR algorithm is comparable to that of the conventional LS method. However, at step size 9, the LS method begins to show noticeably higher reconstruction error compared to LSQR, and at step size 10, a sharp increase in RMSE occurs, indicating the onset of ill-conditioning. Beyond step 10, the RMSE exceeds 10, signifying complete deviation from acceptable accuracy. In contrast, the LSQR method continues to yield reliable current reconstructions, demonstrating strong numerical stability. In terms of solution time, the difference between the two methods remains within 2 seconds across all step sizes, and this difference decreases as the extraction step increases.

A closer examination of Fig. 3 (b) reveals that the overall solution time is significantly reduced due to the decreased number of constructed CMs. Owing to the higher-quality CMs obtained through the dual screening strategy, the conditioning of the LS solver is notably improved. Consequently, the RMSE values for both reconstruction methods remain nearly identical within the extraction step range of 4 to 14. Slight ill-conditioning only begins to appear when the extraction step exceeds 18 for the LS algorithm, and noticeable ill-conditioning appears only when the step size reaches 20. Overall, the reconstruction stability is further enhanced, while the difference in solution time remains negligible.

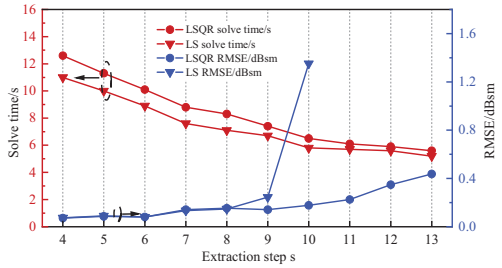

(a)

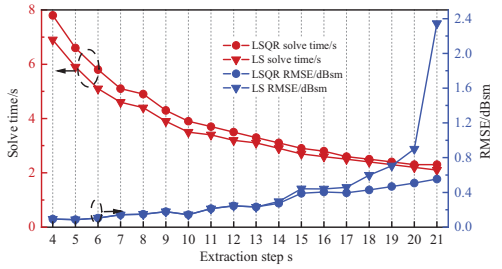

(b)

Fig. 3. Time and RMSE for different extraction steps of the cube model: (a) mathematical screening and (b) dual screening based on mathematical and physical.

Table 2 presents the correlation coefficients between the sparse basis matrix $\mathbf{J}^{CM}$ and the measurement matrix $\hat{\mathbf{Z}}$ constructed using both the CM-CS-MoM and the proposed method. It is evident that the sparse basis matrix $\mathbf{J}^{CM}$ generated by the proposed approach exhibits weak correlation with the sparse sensing matrix $\boldsymbol{\Theta}$ that satisfies the RIP [20], thereby ensuring accurate reconstruction of the current coefficients $\boldsymbol{\alpha}$.

Table 2: Correlation coefficients between measurement matrix and sparse basis matrix

Method	CM-CS-MoM	Proposed method
Coefficient	−0.0075–0.0931i	−0.0034+0.0859i

To further validate the accuracy of the proposed method, Fig. 4 presents a comparison of current distributions obtained using the proposed approach and the conventional MoM. The currents depicted correspond to common border currents uniformly sampled with a step size of 150. Figures 4 (a) and (b) illustrate the

real and imaginary components of the current, respectively. As observed, the reconstructed currents from the proposed method closely align with those computed by MoM, confirming its effectiveness in current recovery. Additionally, Fig. 5 displays the RCS results obtained using both the CM-CS-MoM and the proposed method, with an extraction step size of 5. The RCS values for the horizontally polarized cube calculated using the proposed method show excellent agreement with those produced by MoM, further demonstrating the method's reliability.

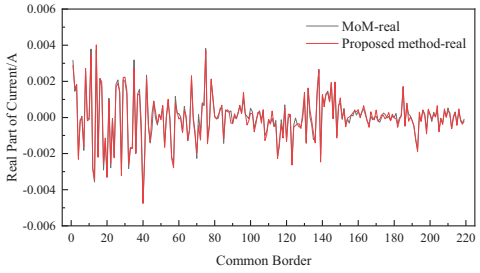

(a)

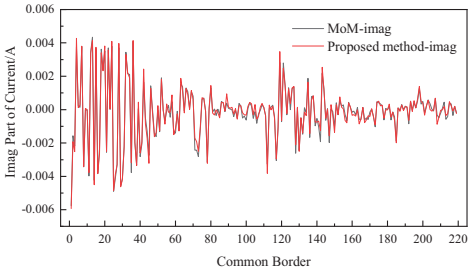

(b)

Fig. 4. Common border currents: (a) current real part and (b) current imaginary part.

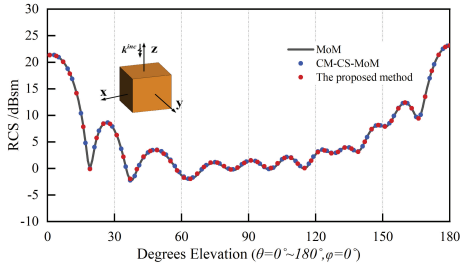

Fig. 5. Bistatic RCS of the cube in horizontal polarization.

Second, to further validate the effectiveness of the proposed method, the bistatic RCS of a 1-meter-long missile target was calculated under plane wave excitation at 4.5 GHz frequency. The incident wave direction was defined as angle $(\theta,\varphi) = (0^\circ,0^\circ)$, while the observation angle was denoted as angle $(\theta,\varphi) = (0^\circ - 360^\circ,0^\circ)$. The target surface was discretized into 36510 triangles, generating 54765 unknowns through RWG basis function discretization. These unknowns were distributed across 16 computational blocks. Furthermore, with an extension width of 0.15 wavelength applied in the computation, the total number of extended unknowns reached 87729.

In this case, the mathematical filtering approach generated a total of 5115 CMs. In contrast, the proposed method incorporated an additional physical screening constraint. Considering the saturation of computational accuracy and solution efficiency, the number of CMs per subdomain is limited to 180, resulting in a total of 2880 CMs. With the extraction step set to 5, Fig. 6 presents the RCS results reconstructed using LS and LSQR for both methods. As illustrated, the results produced by the proposed method exhibit excellent agreement with those obtained from the MoM, demonstrating high computational accuracy.

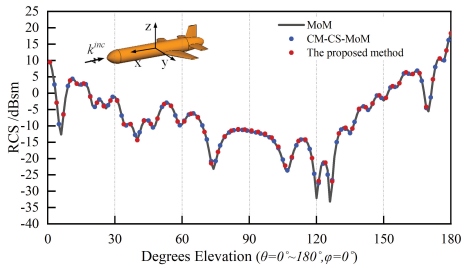

Fig. 6. Bistatic RCS of the missile in horizontal polarization.

Third, to further demonstrate the effectiveness of the proposed method in analyzing electrically large targets, an array composed of 36 PEC objects with two distinct geometries was selected for scattering simulation. The frequency of the incident plane wave was set to 800 MHz, and the scattering was observed at angle $(\theta,\varphi) = (0^\circ - 360^\circ,0^\circ)$. The surface of the array was discretized using RWG basis functions, resulting in a total of 51984 triangular elements and 77976 unknowns. The entire target was partitioned into 36 blocks.

In this case, the conventional mathematical screening method generated a total of 8582 CMs. Using the dual screening strategy combining mathematical and physical constraints and considering the saturation of computational accuracy and solution efficiency, the number of CMs per subdomain is set to 120, resulting in a total of 4320 CMs. Under an extraction step of 6, simulations were performed using both methods, each with LS and LSQR reconstruction, and the results were compared with those obtained by the MoM. As shown in Fig. 7, the proposed method exhibits excellent

Table 3: Simulation time and accuracy

Model	Method	Unknown	CMs Count	Construction Time of Sparse Basis (s)	Recovery Induced Current Time (s)	Total Time (s)	RMSE (dBsm)
Cube	CM-CS-MoM	32832	3196	83.9	9.0	92.9	0.089
	Proposed method		1320	37.8	6.5	44.3	0.087
Missile	CM-CS-MoM	54765	5115	212.5	35.5	248.0	0.221
	Proposed method		2880	136.2	29.0	165.2	0.193
Array Target	CM-CS-MoM	77976	8582	184.3	105.0	289.3	0.365
	Proposed method		4320	99.8	56.6	156.4	0.379

agreement with the MoM results, confirming its high computational accuracy.

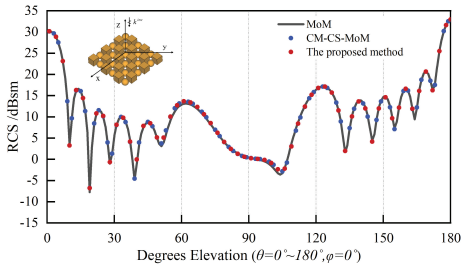

Fig. 7. Bistatic RCS of the array target in horizontal polarization.

Finally, Table 3 presents a comparative analysis of the computational time and RCS error between the CM-CS-MoM method and the proposed method across three different models. It is important to note that the current recovery time includes both the matrix equation construction and current reconstruction phases. As shown in Table 3, under the condition that the RMSE remains nearly the same, the proposed method reduces the number of basis functions by 58.7%, 43.7%, and 49.7%, respectively, compared to CM-CS-MoM. Correspondingly, the total computation time is reduced by 52.3%, 33.4%, and 45.9%, respectively.

IV. CONCLUSION

This paper proposes a dual screening mechanism incorporating physical principles for the construction of CMBFs and employs the LSQR algorithm to achieve efficient reconstruction of current coefficients. By integrating both mathematical and physical screening processes, the approach generates basis functions with higher quality and reduced redundancy, thereby significantly enhancing the efficiency of matrix construction. Meanwhile, the LSQR algorithm demonstrates strong capabilities in handling ill-conditioned matrices, contributing to improved overall computational stability. Simulation results validate that, compared to CM-CS-MoM, the proposed approach exhibits notable advantages in both computational efficiency and stability.

ACKNOWLEDGMENT

This work was supported in part the Natural Science Research Project of Anhui Educational Committee under no. 2022AH051583, in part by the Graduate Innovation Fund of Anhui University of Science and Technology under grant no. 2024cx2062.

REFERENCES

[1] R. F. Harrington, *Field Computation by Moment Methods*. New York: Macmillan, 1968.

[2] J. M. Song and W. C. Chew, "Multilevel fast-multipole algorithm for solving combined field integral equations of electromagnetic scattering," *Microw. Opt. Technol. Lett.*, vol. 10, no. 1, pp. 14–19, Sep. 1995.

[3] E. Lucente, A. Monorchio, and R. Mittra, "An iteration free mom approach based on excitation independent characteristic basis functions for solving large multiscale electromagnetic scattering problems," *IEEE Trans. Antennas Propag.*, vol. 56, no. 4, pp. 999–1007, Apr. 2008.

[4] K. Z. Zhao, M. N. Vouvakis, and J.-F. Lee, "The adaptive cross approximation algorithm for accelerated method of moments computations of EMC problems," *IEEE Trans. Electromagn. Compat.*, vol. 47, no. 4, pp. 763–773, Nov. 2005.

[5] D. L. Donoho, "Compressed sensing," *IEEE Trans. Inf. Theory.*, vol. 52. no. 4, pp. 1289–1306, Apr. 2006.

[6] M. S. Chen, F. L. Liu, H. M. Du, and X. L. Wu, "Compressive sensing for fast analysis of wide-angle monostatic scattering problems," *IEEE Antennas Wireless Propag. Lett.*, vol. 10, pp. 1243–1246, Oct. 2011.

[7] S. R. Chai and L. X. Guo, "Compressive sensing for monostatic scattering from 3-D NURBS geometries," *IEEE Trans. Antennas Propag.*, vol. 64, no. 8, pp. 3545–3553, 2016.

[8] M. Kong, M. S. Chen, X. Y. Cao, L. Zhang, Q. Qi, and X. L. Wu, "Fast analysis of local current distribution for electromagnetic scattering problems of electrically large objects," *IEEE Access*, vol. 8, pp. 127640–127647, July 2020.

[9] M. Kong, M. S. Chen, X. Y. Cao, J. B. Zhu, X. J. Kuang, Q. Qi, and X. L. Wu, "Fast electromagnetic scattering analysis of inhomogeneous dielectric objects over a wide incident angle," *IEEE Antennas Wireless Propag. Lett*., vol. 20, no. 8, pp. 1527–1531, Aug. 2021.

[10] S. R. Chai and L. X. Guo, "Fast analysis of bistatic scattering problems with compressive sensing technique," *J. Electromagn. Waves Appl*., vol. 30, no. 13, pp. 1755–1762, 2016.

[11] M. Kong, M. S. Chen, B. Wu, and X. L. Wu, "Fast and stabilized algorithm for analyzing electromagnetic scattering problems of bodies of revolution by compressive sensing," *IEEE Antennas Wireless Propag. Lett.*, vol. 16, pp. 198–201, May 2017.

[12] Z. G. Wang, H. R. Yuan, Y. F. Sun, W. Y. Nie, and P. Wang, "Block-based Krylov subspace basis functions for solving bistatic scattering problems," *IEEE Antennas Wireless Propag. Lett*., vol. 22, no. 10, pp. 2561–2565, Oct. 2023.

[13] Y. L. Gao, M. F. Akbar, and G. N. Jawad, "Stabilized and fast method for compressive sensing-based method of moments," *IEEE Antennas Wireless Propag. Lett*., vol. 22, no. 12, pp. 2915–2919, Dec. 2023.

[14] P. Wang, Z. G. Wang, Y. F. Sun, and W. Y. Nie, "Novel compressive sensing computing model used for analyzing electromagnetic scattering characteristics of three-dimensional electrically large objects," *Acta Phys. Sin*., vol. 72, no. 3, pp. 54–61, Feb. 2023.

[15] Z. G. Wang, W. Y. Nie, and H. Lin, "Characteristic basis functions enhanced compressive sensing for solving the bistatic scattering problems of three-dimensional targets," *Microw. Opt. Technol. Lett*., vol. 62, no. 10, pp. 3132–3138, May 2020.

[16] Z. G. Wang, P. Wang, Y. F. Sun, and W. Y. Nie, "Fast analysis of bistatic scattering problems for three-dimensional objects using compressive sensing and characteristic modes," *IEEE Antennas Wireless Propag. Lett*., vol. 21, no. 9, pp. 1817–1821, Sep. 2022.

[17] X. Y. Cao, M. S. Chen, Q. Qi, M. Kong, J. H. Hu, L. Zhang, and X. L. Wu, "Solving electromagnetic scattering problems by underdetermined equations and Krylov subspace," *IEEE Microw. Wireless Compon. Lett*., vol. 30, no. 6, pp. 541–544, June 2020.

[18] J. A. Tropp and A. C. Gilbert, "Signal recovery from random measurements via orthogonal matching pursuit," *IEEE Trans. Inf. Theory*., vol. 53, no. 12, pp. 4655–4666, 2007.

[19] J. Wang, S. Kwon, and B. Shim, "Generalized orthogonal matching pursuit," *IEEE Trans. Signal Process*., vol. 60, no. 12, pp. 6202–6216, Sep. 2012.

[20] E. J. Candes, "The restricted isometry property and its implications for compressed sensing," *Comptes Rendus Math*., vol. 346, no. 9/10, pp. 589–592, 2008.

Yang Liu received the B.E. degree from Suzhou University, China, in 2023. He is currently pursuing the M.S. degree at Anhui University of Science and Technology. His current research interests include computational electromagnetics.

Zhonggen Wang received the Ph.D. degree in electromagnetic field and microwave technique from the Anhui University of China (AHU), Hefei, P. R. China, in 2014. Since 2014, he has been with the School of Electrical and Information Engineering, Anhui University of Science and Technology. His research interests include computational electromagnetics, array antennas, and reflect arrays.

Longhui Sun received the B.E. degree from Fuyang Normal University, China, in 2022. He is currently pursuing the M.S degree in Anhui University of Science and Technology. His current research interest lies in the application of Bayesian compressive sensing in electromagnetic scattering.

Wenyan Nie is a professor at Huainan Normal University, China. She received the B.S. and M.S. degrees from Anhui University of Science and Technology in 2007 and 2012, respectively. Her research interests include computational electromagnetic methods, antenna theory and design.